predict tangential velocity decay for a solid-body rotation prematurely, while experimental data show a persistent combined vortex (i.e., combination of a free and forced vortex) profile even at the far downstream location. The discrepancies between the calculations and measurements indicate the deficiency of isotropic eddy viscosity hypothesis used in this level of closure. This discrepancy is also shared by the non-isotropic algebraic stress model (ASM) prediction.[6] As indicated by Sloan et al.,[6] the failure at the downstream location probably has to be resolved by solving the full stress transport equations, with convective and diffusive terms, rather than the abbreviated ASM.

More detailed comparisons, such as centerline mean velocity decay, envelope of the central recirculation zone, turbulence intensities, and the sensitivity of the numerical predictions to the inlet boundary conditions, have been documented in Ref. (9). The preliminary success of this model stems from recognizing that turbulence in swirl flows departs significantly from spectral equlibrium conditions and that the different energy transfer rates for energy-containing eddies and transfer eddies should be modeled separately. However, the multiple-scale model still adopts the isotropic eddy viscosity formulation. To account for anisotropic turbulence, a full Reynolds Stress Model needs to be used. Incorporation of the multiple-scale turbulence model, which takes into account the non-equilibrium spectral energy transfer rate, and a simplified Reynolds stress model should pave a promising avenue for numerical modeling of swirling flows.

Acknowledgment

This work was done while the author held a National Research Council-NASA Research Associateship. Financial support provided by NASA-MSFC and NRC is acknowledged. The comments of Dr. George Fichtl and the reviewers are also gratefully acknowledged.

References

[1]Rodi, W., "Examples of Turbulence Models for Incompressible Flows," *AIAA Journal*, Vol. 20, July 1982, pp. 872-879.

[2]Boysan, F. and Swithenbank, J., *Journal of Fluids Engineering*, Vol. 104, Sept. 1982, pp. 391-392.

[3]Launder, B. E., Pridden, C. H., and Sharma, B. I., "The Calculation of Turbulent Boundary Layers on Spinning and Curved Surface," *Journal of Fluid Engineering*, Vol. 88, March 1977, pp. 231-239.

[4]Rodi, W., "Influence of Buoyancy and Rotation on Equations for the Turbulent Length Scale," *Proceedings of 2nd Symposium on Turbulent Shear Flows*, Imperial College, London, pp. 10.37-10.42, July 1979.

[5]Chen, C. P., "Calculation of Confined Swirling Jets," *Commu. Applied Numerical Methods*, Vol. 2, 1986, pp. 333-338.

[6]Sloan, D, G., Smoot, L. D., and Smith, P. J., "Modeling of Swirl in Turbulent Flow Systems," Paper presented at Combustion Institute Spring Technical Meeting, Southwest Research Institute, San Antonio, TX, April 1985.

[7]Hanjalic, K., Launder, B. E., and Schiestel, R., "Multiple-Time-Scale Concepts in Turbulent Transport Modeling," *Turbulent Shear Flow II*, Springer-Verlag, NY, 1980, pp. 36-49.

[8]Chen, C. P., "Multiple-Scale Turbulence Modeling in Internal Flows," NASA CR-178536, submitted to *Physics of Fluids*, 1985.

[9]Chen, C.P., "Confined Swirling Jet Predictions Using a Multiple-Scale Turbulence Model," NASA CR-178484, Aug. 1985.

[10]Roback, R. and Johnson, B. V., "Mass and Momentum Turbulent Transport Experiments with Confined Swirling Coaxial Jets," NASA CR-168252, 1983.

[11]Dixon, T. F., Truelove, J. S., and Wall, T. F., "Aerodynamic Study on Swirled Coaxial Jets From Nozzles with Divergent Quarls," *Journal of Fluid Engineering*, Vol. 105, June 1983, pp. 197-203.

Analogy for Postbuckling Structural Resistance Capability

Elie Yitzhak* and Menahem Baruch†
Technion—Israel Institute of Technology, Haifa, Israel

Introduction

THE notion of static postbuckling analysis is contradictory. The use of static assumption presumes that accelerations and inertial forces remain inexistent during the loading process. On the other hand, sudden changes in the modes and rates of displacement, followed by different dynamic effects, are to be expected when buckling is about to occur. This contradiction makes questionable the ability of static analysis to provide actual information on postbuckling structural behavior. Therefore, the results usually supplied by static postbuckling analysis (i.e. the forces vs displacements diagrams) must be considered to be no more than estimations of the structure's ability to develop resistance forces when stability disappears.

Arguments similar to those expressed here have led several authors to inspect the possibility of performing dynamic postbuckling analyses in place of static ones.[1-3] The purpose of this Note is to point out that, in addition to the structural behavior history generally expected, it is possible to extract from the dynamic analysis results information such as diagrams of the structural resistance force vs displacement that are equivalent to the static postbuckling ones. In certain simple cases, diagrams from dynamic analyses are identical to those from static analyses. In more complicated cases, they will be different. Logically then, the dynamic analysis force vs displacement diagrams must contain better information about the structural strength capabilities. All of the existing theorems for the behavior of diagrams of static postbuckling analyses must also be valid for the equivalent dynamic analysis diagrams.

Example Case of Structural Instability

As an example, the assumption noted above will be applied to the case of the structural instability of an elastoplastic thin spherical pressure vessel (Fig. 1). This problem has already been treated from a classical static point of view by Durban and Baruch.[4] The static behavior of such a structure is analogous in many aspects to a nonstable postbuckling history without bifurcation. It is noted that the critical point is obtained on the load displacement path when the load reaches its maximum value. (Real structures, due to their imperfections, do not buckle generally by bifurcation and have a similar behavior to the spherical pressure vessel of this example.)

The internal pressure p is supposed to increase as a monotonic function of the time variable t,

$$p=\alpha t \qquad (\alpha=\text{const}) \tag{1}$$

Two different kinds of forces act together against this pressure: the structural resistance ρ, which represents the resultant of the existing membrane stresses σ within the structure, and an inertia pressure q:

$$\rho=2\sigma\frac{h_0+\eta}{r_0+u} \tag{2a}$$

Received Dec. 4, 1984; revision received Jan. 6, 1986.

*Graduate Student, Department of Aeronautical Engineering.
†Professor and Dean, Department of Aeronautical Engineering. Member AIAA.

$$q=\frac{\gamma_0 h_0 r_0^2}{(r_0+u)^2}\ddot{u} \tag{2b}$$

$$p=\rho+q \tag{2c}$$

where h_0 and r_0 are the initial thickness and mean radius of the spherical shell, respectively, γ_0 the initial mass density, and u and η the radial displacement and the thickness variation, respectively (see Fig. 1). In this discussion, friction forces are neglected.

From the elastoplastic stress-strain relations and the equilibrium equations (see Appendix) and considering that the shell mass remains constant, it is possible to obtain the following set of four differential equations:

$$\dot{\rho}=\frac{1-\bar{A}+\bar{B}}{\bar{A}}\frac{v}{r_0+u}\rho \tag{3}$$

$$\dot{\eta}=\frac{\bar{B}}{\bar{A}}\frac{h_0+\eta}{r_0+u} \tag{4}$$

$$\dot{v}=\frac{(r_0+u)^2}{\gamma_0 h_0 r_0^2}(p-\rho) \tag{5}$$

$$\dot{u}=v \tag{6}$$

where

$$\bar{\rho}=\frac{(r_0+u)}{2(h_0+\eta)E}\rho \tag{7}$$

$$\bar{A}=(1-\nu)\bar{\rho}+\frac{\kappa n K}{2}(\dot{\rho})^n \operatorname{sign}(\dot{\rho}) \tag{8}$$

$$\bar{B}=-2\nu\bar{\rho}-\kappa n K(\bar{\rho})^n\cdot\operatorname{sign}(\bar{\rho}) \tag{9}$$

This set of differential equations has been integrated numerically using a four-stage method of a fourth-order Runge-Kutta classical formula[5] for the following data:

$r_0=400$ mm	$h_0=2.0$ mm
$E=200.0$ GPa	$\nu=0.32$
$k=57{,}800$	$n=3$
$\gamma_0=7640$ kg/m^3	$\alpha=2.6$ GPa/s

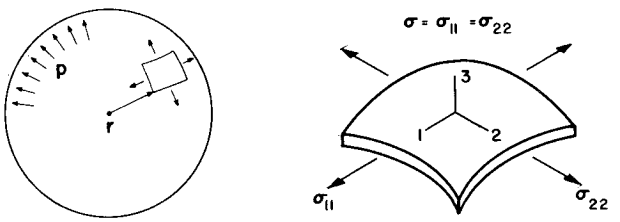

Fig. 1 Thin spherical pressure vessel.

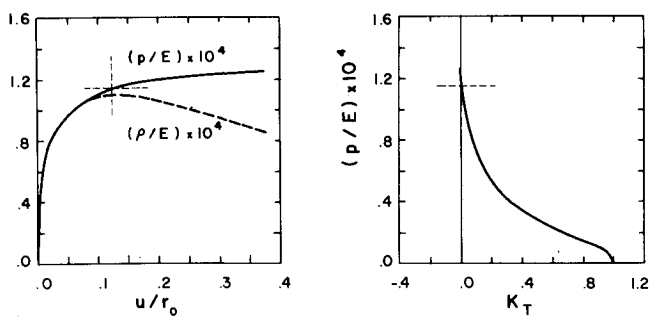

Fig. 2 Dynamic behavior.

The results are the subject of two different curves $p=p(u)$ and $\rho=\rho(u)$ presented in Fig. 2.

It is interesting to note that in this particular case, the curve $\rho=\rho(u)$ obtained via this dynamic analysis is identical to the classical one that can be obtained from static analysis.

Discussion

From the pressure load curve $p=p(u)$, is appears that, after p reaches some critical level, the structural state rapidly becomes unstable. To permit a precise determination of the instability initiation occurence, one has to consider the variation of the other new variable $\rho(u)$. Logically, the structural instability begins when the structural resistance can no longer increase or, in other words, when the tangential stiffness K_T vanishes, as

$$K_T=\left(\frac{d\rho}{du}\right)_{cr}=0 \tag{10}$$

This remark shows the importance of the idea of a simple structural resistance proposed in this Note and ignored until now. Possible extensions of this idea can be suggested along lines parallel to the static stability theorems. For instance, generalizing Eq. (10) for a multiple degree-of-freedom model, the instability initiation can also be defined in the dynamic analysis case as

$$\det|k_{ij}^T|=\det\left|\frac{\partial\rho_i}{\partial u_j}\right|=0 \tag{11}$$

Appendix: Elastoplastic Stress-Strain Relations

The material is assumed to be elastoplastic, obeying the incremental flow theory, and have stress-strain relations of the Ramberg-Osgood type (Fig. A1)

$$\epsilon_e=\frac{\sigma_e}{E}+K\left(\frac{\sigma_e}{E}\right)^n \tag{A1}$$

where ϵ_e and σ_e are the effective strain and stress variables, E the modulus of elasticity, and K and n the Ramberg-Osgood plastic material constants.

According to this classification, the following equation holds:

$$d\epsilon_{ij}=\frac{1}{E}[(1+\nu)d\sigma_{ij}-\nu dI_\sigma\delta_{ij}]+\kappa\frac{3nK}{2E^n}\sigma_e^{n-1}d\sigma_e \tag{A2}$$

where $d\epsilon_{ij}$ and $d\sigma_{ij}$ are the differential stress and strain increments, δ_{ij} is the Kronecker delta, I_σ is the first stress invariant defined as

$$I_\sigma=\sigma_{11}+\sigma_{22}+\sigma_{33} \tag{A3}$$

σ_e is defined as

$$\sigma_e=\left[\frac{3}{2}\left(\sigma_{ij}-\frac{1}{3}I_\sigma\delta_{ij}\right)\left(\sigma_{ij}-\frac{1}{3}I_\sigma\delta_{ij}\right)\right]^{1/2} \tag{A4}$$

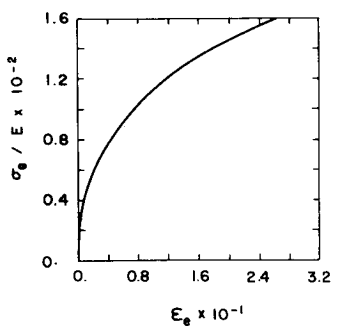

Fig. A1 Ramberg-Osgood stress-strain curve.

ν is the Poisson's ratio, and the parameter κ is defined as

$$\kappa=1 \text{ if } \sigma_e=\sigma_{e_{\max}} \text{ and } d\sigma_e\geq 0$$
$$\kappa=0 \text{ if } \sigma_e<\sigma_{e_{\max}} \text{ or if } \sigma_e=\sigma_{e_{\max}} \text{ and } d\sigma_e<0 \quad \text{(A5)}$$

The static equilibrium equations are

$$\sigma_{11}=\sigma_{22}=\rho r/2h \quad \text{and} \quad \sigma_{33}=0 \quad \text{(A6)}$$

Acknowledgment

The authors would like to thank Dr. J. Ari-Gur and R. D. Richard for helpful suggestions on this work. This work is part of a doctoral thesis by the first author that is to be submitted to the Senate of Technion—Israel Institute of Technology.

References

[1]Hoff, N.J., "Dynamic Stability of Structures," *Dynamic Stability of Structures,* edited by G. Herman, Pergamon Press, New York, 1967.

[2]Vyrlan, P.M. and Shil'krut, D.L., "Stability of Equilibrium Forms of Geometrically Nonlinear Spherical Shells," *Izvestiya Akademii Nauk SSSR, Mekhanika Tverdogo Tela,* Vol. 13, No. 4, 1978, pp. 170-176.

[3]Ginsburg, S. and Gellert, M., "Numerical Solution of Static and Dynamic Nonlinear Multi-Degree-of-Freedom Systems," *Computer Methods in Applied Mechanics and Engineering,* Vol. 23, 1980, pp. 111-125.

[4]Durban, D. and Baruch, M., "Elastic-Plastic Behavior of a Spherical Membrane under Internal Pressure," *Israel Journal of Technology,* Vol. 12, 1974, pp. 23-30.

[5]Gear, C.W., *Numerical Initial Value Problems in Ordinary Differential Equations,* Prentice-Hall, Englewood Cliffs, NJ, 1971.

Buckling of Composite Plates Using Shear Deformable Finite Elements

Frank Kozma*
LTV Corporation, Dallas, Texas
and
Ozden O. Ochoa†
Texas A&M University, College Station, Texas

Introduction

THE instability problem of a composite plate is more complicated than that of an isotropic plate due to the orthotropic properties of each lamina. The focus of this Note is the utilization of a recently developed shear deformable, composite plate element, QHD40, within a finite element program to solve for the critical buckling loads.[1,2] The effort is noteworthy in that the displacement field used in formulation of the composite plate element contains higher-order terms. This allows a more refined model for the stress distribution within the structure, a progression of previous work relating to shear deformation in isotropic and anisotropic plate structures.[2-5] Ochoa et al.[1] presented the results of the eigenvalue problem for the vibration of composite plates using this element. Herein the critical buckling loads for composite plates are calculated and compared to currently available numerical finite element methods (FEM) and analytical results with various fiber orientations and boundary support conditions.[6-8]

Received March 27, 1985; revision received Feb. 20, 1986.

*Structures Engineer, Structural Technology Group, Vought Aero Products Division.

†Assistant Professor, Department of Mechanical Engineering. Member AIAA.

Stability Problem

The stability problem can be formulated in a manner analogous to the standard eigenvalue problem. This can be expressed in matrix notation as

$$([K]\{u\}=-\lambda[KG])\{u\} \quad (1)$$

where $[K]$, λ, $[KG]$, and $\{u\}$ are the stiffness matrix, the lowest eigenvalue (loading), the geometric or initial stiffness matrix, and the eigenvector of nodal displacements corresponding to an eigenvalue, respectively. The solution procedure for Eq. (1) can be summarized as follows:

1) Evaluate stiffness matrix $[K]$ for the chosen element

$$[K]=\int_{\text{vol}}[B]^T[D][B]dV \quad (2)$$

2) Solve for displacements $\{u\}$ by decomposition and back substitution and calculate the stresses.

3) Evaluate the geometric stiffness matrix $[KG]$.

After formulation of the geometric stiffness matrix, the lowest eigenvalue is solved for by the inverse iteration method. Having solved for $\{u_{i+1}\}$ by back substitution, $\{u_{i+1}\}$ is normalized to $\{un_{i+1}\}$, where

$$\{un_{i+1}\}=\{u_{i+1}\}/\lambda_{i+1} \quad (3)$$

The test for convergence is stated as

$$|(|un_{i+1}|-|un_i|)|<e \quad (4)$$

where e is a prescribed value. After convergence, λ_i is obtained by taking the inverse of the value used to normalize $\{u_i\}$. For comparison with previously published results, the following nomenclature is introduced:

$$N_x=\lambda_i/B \quad (5)$$

where N_x and B are the critical buckling load per unit length and width of the plate, respectively.

Element Description

QHD40 is an eight noded quadrilateral plate element with seven degrees of freedom at each corner node and three degrees of freedom per midside node for use in linear/nonlinear applications. The element and associated finite element routines were developed by Engblom and Ochoa.[1,2] The assumed displacement field of the element is

$$u(x,y,z)=u_0(x,y)+z\Psi_x(x,y)+z^2\phi_x(x,y)$$
$$v(x,y,z)=v_0(x,y)+z\Psi_y(x,y)+z^2\phi_y(x,y)$$
$$w(x,y,z)=w_0(x,y) \quad (6)$$

The neutral surface displacements are represented by u_0, v_0, and w_0, the rotation about the y axis is given by Ψ_x, and the rotation about the x axis is denoted by Ψ_y. Coefficients of z^2, ϕ_x, and ϕ_y can be interpreted as contributions from transverse deformations. In-plane displacements (u_0, v_0) and the higher-order terms (ϕ_x, ϕ_y) are expanded in bilinear form as

$$[1\ x\ y\ xy]\{\alpha\} \quad (7)$$